

Coupled control of the horizontal and vertical plane motions of a semi-submersible platform by a dynamic positioning system

Haizhi Liang¹ · Luyu Li² · Jinping Ou^{2,3}

Received: 18 May 2014 / Accepted: 1 May 2015 / Published online: 28 May 2015
© JASNAOE 2015

Abstract Due to the small-waterplane-area of a semi-submersible platform, not only are the surge and sway responses affected by the roll and pitch damping, but also roll and pitch motions may be induced by the propeller activity of the dynamic positioning (DP) system. The coupling characteristics of the dynamic responses between the degrees-of-freedom (DOFs) of the horizontal plane and the vertical plane can no longer be neglected. Therefore, traditional DP control strategies based on the horizontal DOFs are not suitable for the DP of a semi-submersible platform. The Cummins equation is widely used to simulate the response in the time domain. This equation, in which the convolution integral terms are replaced by the state-space model, is directly used to design the DP control strategy used in this study. The advantage of this model is that the coupling effects of the horizontal plane motions and vertical plane motions are considered. Because the sensors can only measure the dynamic motions of the platform, a static output feedback controller using L_∞ performance is designed to reject persistent environmental disturbances for the fully coupled dynamic model. Lyapunov function-based stability analysis is used to guarantee the stability.

Finally, simulation results in the time domain are provided to specify the proposed controller design.

Keywords Semi-submersible platform · Dynamic positioning · State-space model · L_∞ controller · Static output feedback control

1 Introduction

Dynamic positioning (DP) systems have been widely used to keep the floating offshore structures at specified points or to track predefined paths in deep water since their appearance in the 1960s. The core of a DP is its control strategy design that is divided into high-level plant control and low-level thruster control [1]. The models for the description of motion of the floating offshore structures are the basis of designing the DP high-level plant control [2]. In order to reduce wear and tear of propellers, only the low frequency drift motions in the horizontal plane, such as surge, sway, and yaw, are controlled by the DP ([3–8]). And the linear model is built to describe the low frequency drift motions for the DP controller and the wave frequency motion is modeled by separate harmonic oscillators with a variable frequency [9]. However, the semi-submersible platforms' water plane area is small and the hydrostatic restoring forces are low compared with inertial forces [10]. As a result, the vertical plane motions, especially roll and pitch, will be invoked by the DP because of coupling between the vertical and horizontal plane DOFs. Therefore, both the horizontal and vertical plane motions should be considered for the semi-submersible platforms DP controller design.

The Cummins equation [11], which considers fully coupled motions and memory effects, is widely used to

✉ Haizhi Liang
hzliang@mail.dlut.edu.cn

¹ Faculty of Vehicle Engineering and Mechanics, Dalian University of Technology, No. 2 Linggong Road, Ganjingzi District, Dalian 116024, China

² Faculty of Infrastructure Engineering, Dalian University of Technology, No. 2 Linggong Road, Ganjingzi District, Dalian 116024, China

³ State Key Laboratory of Coastal and Offshore Engineering, Dalian University of Technology, No. 2 Linggong Road, Ganjingzi District, Dalian 116024, China

simulate offshore structure dynamic response in the time domain. However, due to the convolution integral terms, it is not straightforward to apply the usual methods for DP controller design. Fortunately, a great deal of research exists regarding state-space representations of the convolution integral terms. In conjunction with calculation of the hydrodynamic frequency dependent added mass and radiation damping, realization theory in the time domain used by Kristiansen and Egeland [12] and Kristiansen et al. [13] and the identification in the frequency domain used by McCabe et al. [14] and Perez and Fossen [2] are applied to this problem. Fossen and Smogeli [15] used this state-space model for the ship low speed maneuvering and station-keeping design. In this paper, this state-space model is adopted for semi-submersible platform to design the DP controller to consider the coupling between the vertical and horizontal plane DOFs.

For DP, high-level plant control design has attracted a great deal of attention. Tannuri et al. [3] proposed an adaptive control strategy to correct controller gains online for a DP. Sliding model control was also proposed by Tannuri et al. [4]. Fossen and Grøvlen [5] applied a backstepping method to design a nonlinear observer with adaptive wave filtering for a DP. Skjetne et al. [6] proposed backstepping control combined with adaptive methods for a model ship. Further, based on the backstepping method, dynamic surface control was applied to a mobile offshore base [7]. For the station-keeping mode, the DP is used to reject the environmental disturbances. To achieve the robustness and the disturbance attenuation, H_∞ feedback control was used for a moored floating platform by Scherer et al. [16]. However, the external disturbances in H_∞ feedback control must satisfy the finite energy condition [17]. For persistent environmental disturbances, the finite energy condition is inapplicable. Instead of H_∞ control, L_∞ optimal control will be a better candidate, which can reject bounded disturbance by consideration for minimizing the maximum amplitude [18–20]. L_∞ optimal control design was used for a wind turbine-induction generator unit by Khosravi and Jalali [21]. Sadeghi et al. [22] also used for a bilateral teleoperation system. In this study, L_∞ optimal control is adopted to design the DP control strategy. To the best of author’s knowledge, it has not been found that L_∞ optimal control is applied for the DP controller design so far.

This paper is organized as follows: Sect. 2 describes the dynamic equations applicable to a semi-submersible platform, where the state-space models replace the convolution integral terms in the Cummins equation. Section 3 describes the design of the static output feedback control using L_∞ performance for the DP controller.

In Sect. 4, simulation results in the time domain are discussed. Since it is undesirable to attempt to counter high frequency motions by the DP, a low pass filter is introduced

to separate the low frequency motion from the overall motion. In addition, the controlled results based on the 3-DOF model using L_∞ optimal control are also shown to compare favorably with the fully coupled model. Finally, Sect. 5 concludes the study.

2 Dynamic models

2.1 Dynamic mathematical equation

The general dynamic equation of the offshore floating structure is given by

$$\sum_{k=1}^6 m'_{jk} \ddot{x}_k = \tau_j^H + \tau_j^R + \tau_j^D + \tau_j^F + \tau_j^{\text{Drift}} + \tau_j^A + \tau_j^M + \tau_j^C + \tau_j^W, \tag{1}$$

where τ_j^H is the hydrostatic force, τ_j^R is the radiation force, τ_j^D is the diffraction force, τ_j^F is the Froude–Krylov force, τ_j^{Drift} is the second order wave force, τ_j^A is the propeller force, τ_j^M is the mooring force, τ_j^C is the current drag force, τ_j^W is the wind drag force, m'_{jk} is the structure mass/inertia, \ddot{x}_k is the acceleration, and j is the corresponding DOF.

Considering the radiation potential memory effects, the Cummins equation [11] based on Eq. 1 is given by

$$\sum_{k=1}^6 \left\{ (M'_{jk} + a_{jk}(\infty)) \ddot{x}_k(t) + \int_{-\infty}^t K_{jk}(t-\tau) \dot{x}_k(\tau) d\tau + B_{jk} \dot{x}_k(t) + C_{jk} x_k(t) \right\} = \tau_j^{\text{wave}} + \tau_j^A + \tau_j^C + \tau_j^W + \tau_j^M, \tag{2}$$

where M'_{jk} is the mass/inertia of the platform, $a_{jk}(\infty)$ is the added mass/inertia of infinite frequency, K_{jk} is the retardation function, B_{jk} is the wave-drift damping coefficient, C_{jk} is the hydrostatic stiffness coefficient, and τ_j^{wave} is the sum of τ_j^D , τ_j^F and τ_j^{Drift} . The added inertial force and radiation damping comprise the radiation forces [23], which are obtained as

$$\tau_j^R = - \sum_{k=1}^6 a_{jk} \ddot{x}_k(t) - \sum_{k=1}^6 \int_{-\infty}^t K_{jk}(t-\tau) \dot{x}_k(\tau) d\tau, \tag{3}$$

and they are calculated from the radiation potential ϕ_R that is given in the convolution integral term as

$$\phi_R(r, t) = \sum_{i=1}^6 \dot{x}_i(t) \psi_i(r) + \sum_{i=1}^6 \int_{-\infty}^t \chi_i(r, t-\tau) \dot{x}_i(\tau) d\tau, \tag{4}$$

where ψ_i is the potential induced by \dot{x}_i , χ_i is the fluid potential that considers memory effects, and they all satisfy certain specific boundary conditions. The irregular waves

are considered as a combination of the regular waves with different frequencies. The first order wave forces are calculated by

$$\tau_j^F + \tau_j^D = \sum_{l=1}^N a_l F_l' \cos(-\omega_l t + \varepsilon_l), \tag{5}$$

where a_l and F_l' are the amplitude of regular wave component and the amplitude of Froude–Krylov and diffraction force corresponding to ω_l of each regular wave component in the spectrum, respectively; ε_l is the random phase angle; N is the number of wave components. The quadratic transfer function (QTF) is adopted to calculate the second order wave-drift force. Neglecting the sum frequency components, the second order wave forces can be written as

$$\begin{aligned} \tau_j^{\text{Drift}} = & \sum_{m=1}^N \sum_{n=1}^N \{ F_{mn}^{\text{in}} \cos[-(\omega_m - \omega_n)t + (\varepsilon_m - \varepsilon_n)] \\ & + F_{mn}^{\text{out}} \sin[-(\omega_m - \omega_n)t + (\varepsilon_m - \varepsilon_n)] \}, \end{aligned} \tag{6}$$

where F_{mn}^{in} and F_{mn}^{out} are the in-phase and out-of-phase components of the time-independent transfer function, they include waterline integral, acceleration, momentum, and second order potential term; ω_m and ω_n are the frequencies of wave components; ε_m and ε_n are the random phase angles; N is the number of wave components.

2.2 State-space representation of radiation damping forces

In the traditional time-domain numerical simulations of the dynamic response, the convolution integral terms are directly calculated. However, it is time consuming and inconvenient to design a control strategy for the DP of a semi-submersible platform based on Eq. 2. In this section, each nonzero convolution integral term in radiation damping matrix can be represented by the state-space model, as

$$\begin{aligned} \dot{\xi} &= \mathbf{A}_\xi \xi + \mathbf{B}_\xi \dot{x}_k \\ \mu_{jk} &= \mathbf{C}_\xi \xi + \mathbf{D}_\xi \dot{x}_k, \end{aligned} \tag{7}$$

where ξ is the state vector, \dot{x}_k is the input consisting of the velocity of the platform, \mathbf{A}_ξ , \mathbf{B}_ξ , \mathbf{C}_ξ , and \mathbf{D}_ξ are state-space matrices that will be determined later, and μ_{jk} is the output of the convolution integral terms. The value of μ_{jk} in Eq. 2 is

$$\mu_{jk}(t) = \int_{-\infty}^t K_{jk}(t - \tau) \dot{x}_k(\tau) d\tau. \tag{8}$$

If we let $\dot{x}_k(\tau) = \delta(\tau)$, where $\delta(\tau)$ is a unit impulse input at $\tau = 0$, $K_{jk}(t)$ becomes an impulse response function. Considering the physical mechanism, $K_{jk}(t)$ must satisfy

$$K_{jk}(t) = 0 \quad t < 0,$$

and the velocity satisfies

$$\dot{x}_k(\tau) = 0 \quad \tau > t.$$

Therefore, the lower limit of the integral in Eq. 8 is replaced by 0. If we let $\dot{x}_k(t)$ be replaced by $u(t)$ as the input signal, the Laplace transforms of the signals $\mu_{jk}(t)$ are

$$\begin{aligned} \tilde{\mu}_{jk}(s) &= L\{\mu_{jk}(t)\} = L\left\{ \int_0^t K_{jk}(t - \tau) u(\tau) d\tau \right\} \\ &= \tilde{K}_{jk}(s) \tilde{u}(s). \end{aligned} \tag{9}$$

Equation (9) therefore becomes

$$\tilde{\mu}_{jk}(s) = \tilde{K}_{jk}(s) \tilde{u}(s), \tag{10}$$

where $\tilde{K}_{jk}(s)$ is the transfer function of the impulse response function and $\tilde{u}(s)$ is the input signal. $\tilde{K}_{jk}(s)$ can be denoted by

$$\tilde{K}_{jk}(s) = \mathbf{C}_\xi (s\mathbf{I} - \mathbf{A}_\xi)^{-1} \mathbf{B}_\xi + \mathbf{D}_\xi. \tag{11}$$

If $K_{jk}(t)$ is calculated in the time domain, the matrices of the state-space model in Eq. 7 will be determined from Eq. 11. The platform is assumed to be forced to do harmonic oscillations $x_k(t) = x_k e^{-i\omega t}$ in regular waves of frequency ω , and $x_k(t) = 0$ for $t \leq 0$. Substituting $x_k(t)$ into Eq. 2, we obtain

$$\begin{aligned} \sum_{k=1}^6 \left\{ -\omega^2 (M'_{jk} + a_{jk}) x_k e^{-i\omega t} - i\omega \int_{-\infty}^t K_{jk}(t - \tau) x_k e^{-i\omega\tau} d\tau \right. \\ \left. - i\omega B_{jk} x_k e^{-i\omega t} + C_{jk} x_k e^{-i\omega t} \right\} = \tau_j^{\text{wave}} + \tau_j^{\text{A}} + \tau_j^{\text{C}} + \tau_j^{\text{W}} + \tau_j^{\text{M}}. \end{aligned} \tag{12}$$

This is equivalent to motion in the frequency domain [24], and we obtain

$$a_{jk}(\omega) = m_{jk} - \frac{1}{\omega'} \int_0^\infty K_{jk}(t) \sin \omega t dt, \tag{13a}$$

$$B'_{jk}(\omega) = b_{jk} + \int_0^\infty K_{jk}(t) \cos \omega t d\omega, \tag{13b}$$

where $a_{jk}(\omega)$ is the frequency dependent added mass, $B'_{jk}(\omega)$ is the frequency dependent radiation damping, m_{jk} and b_{jk} are the added mass and radiation damping of arbitrary frequency. The Fourier transformation of $K_{jk}(t)$ is

$$\hat{K}_{jk}(\omega) = \int_0^\infty K_{jk}(t) \cos \omega t dt - j \int_0^\infty K_{jk}(t) \sin \omega t dt. \tag{14}$$

From the viewpoint of a physical mechanism, the energy of the impulse response function is finite, so $\hat{K}_{jk}(\omega)$ tends to

zero as ω tends to infinity. $K_{jk}(t)$ is obtained from the inverse Fourier transformation of Eq. 14:

$$K_{kj}(t) = -\frac{2}{\pi} \int_0^\infty \omega [a_{kj}(\omega) - m_{kj}] \sin \omega t d\omega, \tag{15a}$$

$$K_{kj}(t) = \frac{2}{\pi} \int_0^\infty [B'_{kj}(\omega) - b_{kj}] \cos \omega t d\omega. \tag{15b}$$

When $K_{jk}(t)$ is calculated, the state space of the convolution integral terms can be obtained using the least square method or realization theory [12, 13].

From the above, Eq. 2 can be rewritten as the dynamic mathematical state-space model:

$$\dot{\mathbf{x}}_s = \mathbf{A}\mathbf{x}_s + \mathbf{B}_u\mathbf{u} + \mathbf{E}\mathbf{w}. \tag{16}$$

In Eq. 16, \mathbf{x}_s is the state vector, $\mathbf{x}_s = [\mathbf{x}^T \ \dot{\mathbf{x}}^T \ \xi^T]^T$, where the superscript T represents the transpose of the matrix and \mathbf{x} is the displacement vector of the six DOFs, $\mathbf{x} = [x \ y \ z \ \theta \ \phi \ \psi]^T$, and $\dot{\mathbf{x}}$ is the velocity vector of the six DOFs. The details of the matrices in Eq. 16 are given below, for $\mathbf{M} = \mathbf{M}' + \mathbf{a}$, where \mathbf{M}' is the inertia matrix and \mathbf{a} is the inertia matrix of added mass terms, \mathbf{C} is the hydrostatic matrix, \mathbf{B} is the wave-drift damping matrix which is calculated based on the AQWA, \mathbf{w} is the total environmental disturbance vector, $\mathbf{w} = \tau^C + \tau^W + \tau^{wave}$, \mathbf{u} is the control force vector, $\mathbf{u} = \tau^A$, and \mathbf{H} is the control input transfer matrix that must be included because only horizontal plane control forces (moments) are generated by the propellers. In this study, only the dynamic positioning system is equipped, and the mooring forces are neglected. And the velocity of the semi-submersible platform of the station-keeping mode is around zero and the viscous damping is neglected [25].

$$\begin{aligned} \mathbf{A} &= \begin{bmatrix} 0 & I & 0 \\ -\mathbf{M}^{-1}\mathbf{C} & -\mathbf{M}^{-1}\mathbf{B} + \mathbf{D}_\xi & -\mathbf{M}^{-1}\mathbf{C}_\xi \end{bmatrix}, \mathbf{B}_u \\ &= \begin{bmatrix} 0 & \mathbf{B}_\xi & \mathbf{A}_\xi \\ \mathbf{M}^{-1}\mathbf{H} & \mathbf{H} & \mathbf{0} \end{bmatrix}^T, \mathbf{H} = \begin{bmatrix} 1 & 0 & 0 & 0 & 0 & 0 \\ 0 & 1 & 0 & 0 & 0 & 0 \\ 0 & 0 & 0 & 0 & 0 & 1 \end{bmatrix} \\ &= \begin{bmatrix} 0 \\ \mathbf{M}^{-1} \\ 0 \end{bmatrix}. \end{aligned}$$

3 L_∞ control design for the horizontal and vertical plane DOF coupled model

To achieve excellent control performance for a semi-submersible platform using a DP, peak-to-peak gain performance is considered in the design of the DP controller, as described in this section. This control strategy design defines a map between the bounded amplitude inputs and the bounded amplitude outputs. Using the forward difference method, a discrete model based on Eq. 16 is given by

$$\mathbf{x}(k+1) = \mathbf{A}^d\mathbf{x}(k) + \mathbf{B}_u^d\mathbf{u}(k) + \mathbf{E}^d\mathbf{w}(k). \tag{17}$$

Considering the measurement sensors of the platform, only the displacements in the state vector $\mathbf{x}(k)$ can be measured. Therefore, the displacements are taken as the output in this study, given as

$$\mathbf{y}(k) = \mathbf{C}_1\mathbf{x}(k), \tag{18}$$

where $\mathbf{C}_1 = [I_{6 \times 6} \ \mathbf{0}]$. Correspondingly, the static output feedback controller is proposed as

$$\mathbf{u}(k) = \mathbf{K}\mathbf{y}(k), \tag{19}$$

where \mathbf{K} is the feedback control gain. The DP can only control the horizontal plane motions, so that the controlled output states are the displacements of surge, sway, and yaw, as

$$\mathbf{z}(k) = \mathbf{C}_2\mathbf{x}(k), \tag{20}$$

where $\mathbf{C}_2 = [\mathbf{C}_z \ \mathbf{0}]$ for

$$\mathbf{C}_z = \begin{bmatrix} 1 & 0 & 0 & 0 & 0 & 0 \\ 0 & 1 & 0 & 0 & 0 & 0 \\ 0 & 0 & 0 & 0 & 0 & 1 \end{bmatrix}.$$

Substituting Eq. 19 into 17, the closed-loop system becomes

$$\mathbf{x}(k+1) = (\mathbf{A}^d + \mathbf{B}_u^d\mathbf{K}\mathbf{C}_1)\mathbf{x}(k) + \mathbf{E}^d\mathbf{w}(k). \tag{21}$$

The optimal L_∞ control problem is to specify the control input $\mathbf{u}(k)$ such that the following relationship is achieved for the closed loop system of Eq. 21:

$$\frac{\|\mathbf{z}(k)\|_\infty}{\|\mathbf{w}(k)\|_\infty} < \gamma \quad \mathbf{w}(k) \in L_\infty. \tag{22}$$

The results of the L_∞ control synthesis are summarized in following theorem:

Theorem 1 *Considering the system given by Eq. 17 with the static output feedback control given in Eq. 18, for a given positive scalar $\gamma > 0$, the close-loop system Eq. 21 is*

robust stable and the L_∞ induced norm of the system is less than γ if there exist a symmetric positive definite matrix \mathbf{Q} and positive λ and μ such that

$$\begin{bmatrix} -\mathbf{Q} + \lambda\mathbf{Q} & * & * \\ 0 & -\mu\mathbf{I} & * \\ (\mathbf{A}^d + \mathbf{B}_u^d\mathbf{K}\mathbf{C}_1)\mathbf{Q} & \mathbf{E}^d & -\mathbf{Q} \end{bmatrix} < 0, \tag{23}$$

$$\begin{bmatrix} \lambda\mathbf{Q} & * & * \\ 0 & (\gamma - \mu)\mathbf{I} & * \\ \mathbf{C}_2\mathbf{Q} & 0 & -\gamma\mathbf{I} \end{bmatrix} > 0, \tag{24}$$

then the system comprising (17) and (20) satisfies the relationship

$$\|\mathbf{z}(k)\|_\infty < \gamma^2 \|\mathbf{w}(k)\|_\infty. \tag{25}$$

Proof [18, 22, 26] Let us consider the Lyapunov function for the system given by Eq. 21:

$$V_{k+1} = |\mathbf{P}^{1/2}\mathbf{x}(k+1)|^2 = \mathbf{x}^T(k+1)\mathbf{P}\mathbf{x}(k+1), \tag{26}$$

where \mathbf{P} is the symmetric positive definite matrix. Substituting Eq. 21 into Eq. 26 yield

$$\begin{aligned} V_{k+1} &= [(\mathbf{A}^d + \mathbf{B}_u^d\mathbf{K})\mathbf{x}(k) + \mathbf{E}^d\mathbf{w}(k)]^T \mathbf{P} [(\mathbf{A}^d + \mathbf{B}_u^d\mathbf{K})\mathbf{x}(k) + \mathbf{E}^d\mathbf{w}(k)] \\ &= \begin{bmatrix} \mathbf{x}(k) \\ \mathbf{w}(k) \end{bmatrix}^T \begin{bmatrix} (\mathbf{A}^d + \mathbf{B}_u^d\mathbf{K})^T \mathbf{P} (\mathbf{A}^d + \mathbf{B}_u^d\mathbf{K}) + \lambda\mathbf{P} & (\mathbf{A}^d + \mathbf{B}_u^d\mathbf{K})^T \mathbf{P} \mathbf{E}^d \\ (\mathbf{E}^d)^T \mathbf{P} (\mathbf{A}^d + \mathbf{B}_u^d\mathbf{K}) & (\mathbf{E}^d)^T \mathbf{P} \mathbf{E}^d - \mu\mathbf{I} \end{bmatrix} \begin{bmatrix} \mathbf{x}(k) \\ \mathbf{w}(k) \end{bmatrix} \\ &\quad - \lambda\mathbf{x}^T(k)\mathbf{P}\mathbf{x}(k) + \mu\mathbf{w}^T(k)\mathbf{w}(k) \end{aligned} \tag{27}$$

The forward difference of V_k is

$$\Delta V = V_{k+1} - V_k. \tag{28}$$

If we let $\mathbf{P} = \mathbf{Q}^{-1}$, pre-multiply and post-multiply both sides of Ineq. 23 by $\text{diag}([\mathbf{P} \ \mathbf{I} \ \mathbf{P}])$, and use the Schur complement [27], the inequality becomes

$$\begin{bmatrix} (\mathbf{A}^d + \mathbf{B}_u^d\mathbf{K})^T \mathbf{P} (\mathbf{A}^d + \mathbf{B}_u^d\mathbf{K}) + \lambda\mathbf{P} - \mathbf{P} & (\mathbf{A}^d + \mathbf{B}_u^d\mathbf{K})^T \mathbf{P} \mathbf{E}^d \\ (\mathbf{E}^d)^T \mathbf{P} (\mathbf{A}^d + \mathbf{B}_u^d\mathbf{K}) & (\mathbf{E}^d)^T \mathbf{P} \mathbf{E}^d - \mu\mathbf{I} \end{bmatrix} < 0. \tag{29}$$

Therefore, if Ineq. 23 is satisfied, Ineq. 29 holds, and Eq. 28 also satisfies the following inequality:

$$\Delta V < -\lambda\mathbf{x}^T(k)\mathbf{P}\mathbf{x}(k) + \mu\mathbf{w}^T(k)\mathbf{w}(k). \tag{30}$$

When $\mathbf{x}^T(k)\mathbf{P}\mathbf{x}(k) > \frac{\mu}{\lambda}\mathbf{w}^T(k)\mathbf{w}(k)$, $\Delta V < 0$ holds. Under the zero initial conditions $\mathbf{x}(0) = 0$, the following condition is obtained:

$$V_k < \frac{\mu}{\lambda}\mathbf{w}^T(k)\mathbf{w}(k). \tag{31}$$

Pre-multiplying and post-multiplying both sides of Ineq. 24 by $\text{diag}([\mathbf{P} \ \mathbf{I} \ \mathbf{I}])$ and using the Schur complement yield

Table 1 Specifications of HYSY-981

Quantity	Unit	Value
Mass	t	53140
Pontoon length	m	114.07
Pontoon width	m	20.12
Pontoon height	m	8.60
Column length	m	17.38
Column width	m	17.38
Column height	m	21.46
Vertical center of gravity ^a	m	5.8
Draft	m	19
Water depth	m	1500

^a Measured from waterline

$$\frac{1}{\gamma} \begin{bmatrix} \mathbf{C}_2^T \\ 0 \end{bmatrix} [\mathbf{C}_2 \ 0] < \begin{bmatrix} \lambda\mathbf{P} & 0 \\ 0 & (\gamma - \mu)\mathbf{I} \end{bmatrix}. \tag{32}$$

Pre-multiplying and post-multiplying both sides of Ineq. 32 by $[\mathbf{x}^T(k) \ \mathbf{w}^T(k)]$, yield

$$\frac{1}{\gamma}\mathbf{x}^T(k)\mathbf{C}_2^T\mathbf{C}_2\mathbf{x}(k) - (\gamma - \mu)\mathbf{w}^T(k)\mathbf{w}(k) - \lambda V_k < 0. \tag{33}$$

Considering Ineq. 31, we obtain

$$\begin{aligned} \frac{1}{\gamma}\mathbf{x}^T(k)\mathbf{C}_2^T\mathbf{C}_2\mathbf{x}(k) - \gamma\mathbf{w}^T(k)\mathbf{w}(k) \\ = \frac{1}{\gamma}\mathbf{z}^T(k)\mathbf{z}(k) - \gamma\mathbf{w}^T(k)\mathbf{w}(k) < 0. \end{aligned} \tag{34}$$

By taking the supremum for Ineq. 34 over $k > 0$, the L_∞ gain of (22) is derived.

Applying the static output feedback control, Ineq. 23 is the bilinear matrix inequality (BMI), which is the no convex formulation. In this study, the YALMIP packages [28] are employed to solve the linear matrix inequalities (LMIs) using the PENBMI solver [29] within the Matlab environment.

For the system given by Eq. 17, due to the additional state vectors of the convolution integral terms, the dimension of the total states is very large. If the number of scalar entries in the Lyapunov matrix \mathbf{P} is significantly larger than the output matrix \mathbf{K} , the task will be computationally prohibitive [30]. To solve this problem, the balanced truncation algorithm is used to reduce the order of the state-space model.

4 Numerical results

The HYSY-981 semi-submersible platform is adopted in this study. The main structure of this platform consists of two pontoons, four columns, deck, and derrick. The specifications of the HYSY-981 are presented in Table 1.

4.1 Identification of the convolution model

The frequency dependent hydrodynamic parameters are calculated using the ANSYS AQWA software. The hydrodynamic panel model of the semi-submersible platform underwater geometry is given in Fig. 1. The frequencies are ranged from 0.1 to 3.5 rad/s with 0.025 rad/s steps. To obtain very high frequency radiation damping, 7960 panel elements are chosen.

From the radiation damping matrix \mathbf{B}' shown below, it can be seen that there are 10 non-zero parameters because of the symmetrical underwater geometry about the x - z plane. Several typical results of hydrodynamic coefficients are given to describe the state-space model of the convolution integral terms. The radiation damping results of B'_{22} and B'_{24} in the frequency domain, which are the sway and sway-roll coupled terms, are shown in Fig. 2a, b, respectively.

The time series of the impulse response function $K(t)$ is calculated from Eq. 15a. Subsequently, the realization theory is applied to estimate the matrices of the state-space model. This method has been packaged in the robust control toolbox of Matlab as the function `imp2ss`. The convolution integral terms yield a high order state-space model from `imp2ss`, where the order is proportional with

the simulation time length. However, it is inconvenient to design a controller with respect to such a high order model. Therefore, a reduction method employing the balanced truncation algorithm is used to obtain a lower order state-space model. The results for B'_{22} and B'_{24} from the state-space model are shown in Fig. 3 for the different state-space model orders. In Fig. 3, K_{22} and K_{24} are the original dates calculated from Eq. 15a, b. It can be seen that the results from the 10th-order state-space model is better than the other results. However, with consideration for computational efficiency, the 2nd-order model is thought to be sufficiently accurate to simulate the convolution integral terms.

4.2 Time-domain numerical simulation

For simulations, the operational conditions for the HYSY-981 in the South China Sea are adopted. Irregular waves are provided by the JONSWAP spectrum with a significant wave height of 6.0 m, a peak period of 11.2 s, and a peak enhancement factor of 2.0. The time histories of wave forces including first wave force and drift force are given in Fig. 4. And the power spectral density (PSD) of the surge wave force is given in Fig. 5.

Fig. 1 The hydrodynamic panel model of the semi-submersible platform

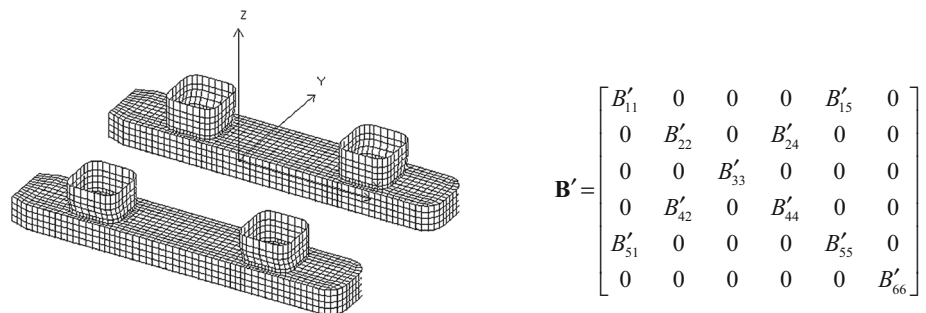


Fig. 2 Radiation damping of B'_{22} and B'_{24} in the frequency domain

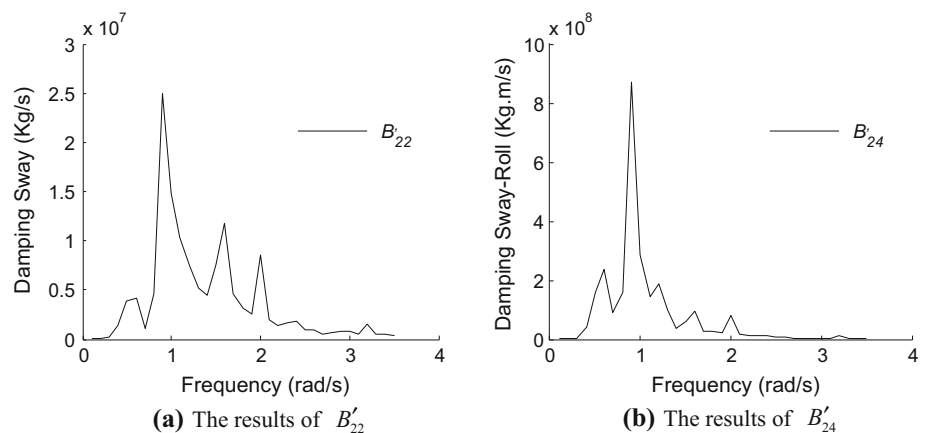


Fig. 3 Impulse response of B'_{22} and B'_{24}

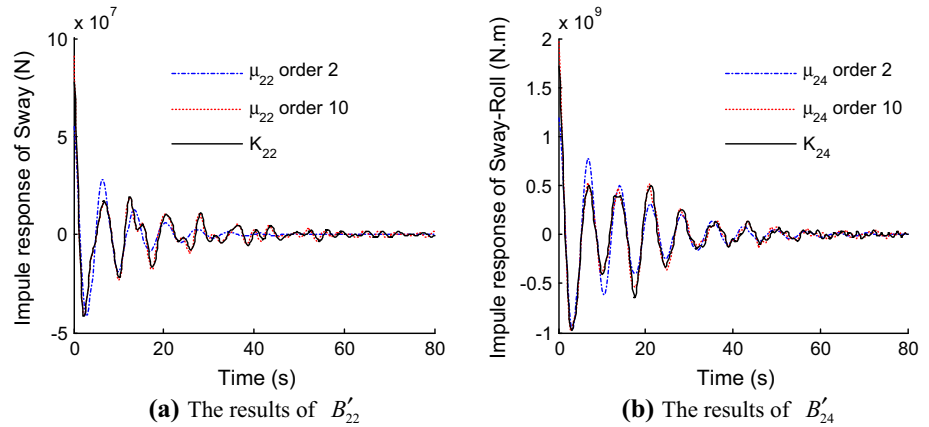


Fig. 4 Time histories of wave forces of surge DOF

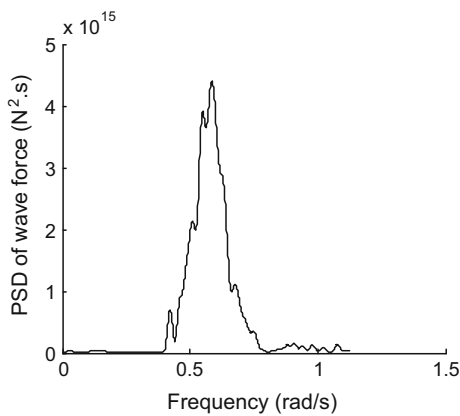
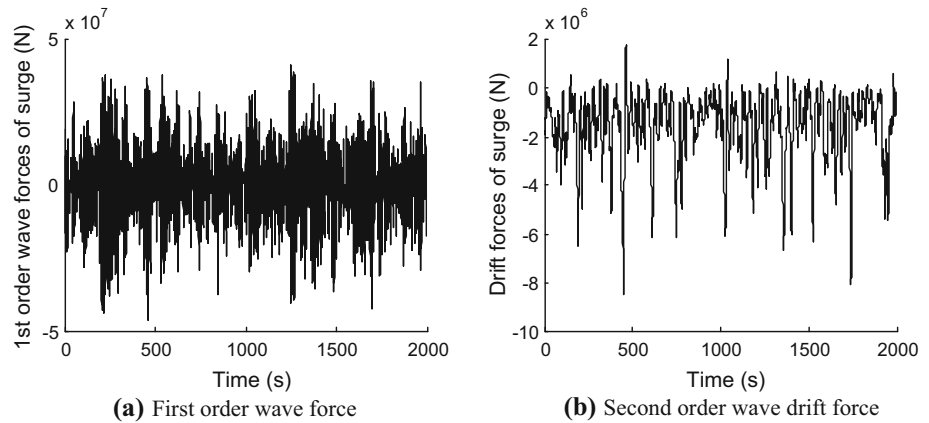


Fig. 5 PSD of surge wave force

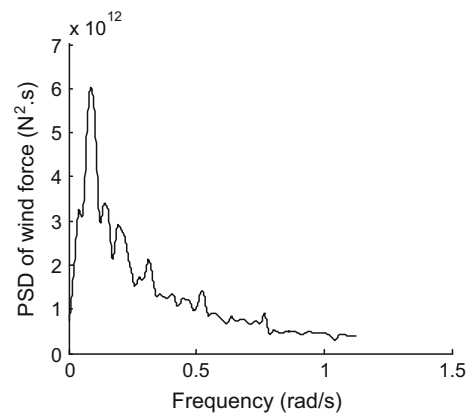


Fig. 6 PSD of surge wind force

The Ochi-Shin wind spectrum is used to simulate the wind forces. The wind velocity at a reference height of 10 m for 1 min is 23.2 m/s. The PSD of the surge wind force is given in Fig. 6. The surface current velocity is 0.9 m/s. The current forces are calculated by the Morison equation. Wave, wind, and current forces are collinear, from a direction 135° measured clockwise from the positive x -axis. The coefficients of hydrostatic matrix and

wave-drift damping matrix are determined by AQWA and experimental results [31]. The 3 h' time domain simulations are carried out in the MATLAB with 0.2 s time increment.

To design the controller, six DOFs displacements are adopted as the measured output, and the horizontal displacements of surge, sway, and yaw are the controlled output. It is found that, when $\mu = 5 \times 10^4$ and

$\lambda = 1 \times 10^{-4}$, a feasible solution of Theorem 1 yields the output feedback controller. The positioning target is set to be the coordinate origin, and the heading angle is zero degree. The platform position is shown in Fig. 7a. The platform moves from the initial zero point under the environmental loads, and is restrained to a limited range by the DP. It can be seen that the horizontal plane displacements are less than 2.5 % of the water depth, which is the positioning requirement [32]. The time histories of roll, pitch, and yaw from 1,500 s to 2,000 s are shown in Fig. 7b. The yaw motion is between $\pm 0.5^\circ$ and satisfies the operational positioning requirement.

The time histories of the control forces and moments from 1,500 to 2,000 s are given in Fig. 8a, b, respectively. To analyze the frequency components of the control forces, the PSD of the surge control force is given in Fig. 9. With consideration for propeller wear and tear, it is ideal that only the low frequency control forces are generated by the propellers, and only the large amplitude drift motions are controlled by the DP. In this study, although the total motion comprises the measured output, it can also be seen that the main frequency components are still distributed in the low frequency range because the large amplitude drift motions are the main components in the measured output. Figure 10 shows the surge radiation damping force calculated via the state-space model, and it is the sum of the diagonal term for surge and the coupling term between surge and pitch in \mathbf{B}' .

To compare our results with those of the traditional controller design that is only used to control low frequency motion, a first order low pass filter [33] is adopted to separate the low frequency motion from the total motion. The first order low pass filter in the time domain is

$$\dot{x}_l + \omega_c x_l = \omega_c x,$$

where x_l is the filtered signal, ω_c is the cut-off frequency, and x is the total signal which contains both high frequency and low frequency components. The horizontal plane motions of the platform, such as surge, sway, and yaw, are thereby filtered in the controller design. After introducing the low pass filter, the system state vector of Eq. 16 becomes $x_{s,l} = [x^T \quad \dot{x}^T \quad \xi^T \quad x_l^T]^T$ and the matrices are accordingly augmented. To design the controller, the measured outputs are the filtered horizontal motions and other vertical plane motions, and the filtered horizontal displacements of surge, sway, and yaw are the controlled outputs.

In this study, the cut-off frequency is set to be 0.2 rad/s which is larger than the lower limit of the bandwidth of DP system to be much safer for the propellers to avoid wear and tear. To illustrate the effects of the filter for the displacements, the results of the total motion and filtered motion of surge are given in Fig. 11. It can be seen that the high frequency components of surge displacements are attenuated. The filtered horizontal plane displacements and other vertical plane displacements as the feedback states are used to form the feedback controller. To compare the control performances, two cases' results, one is with filter and the other is without filter, are given at the same time. For comparison purpose, the maximum amplitudes of the control forces for the two cases are designed to be equivalent via the parameter tuning as shown in Fig. 12. Under these control forces, the displacement of surge is given in Fig. 13. It is obviously that the control performance with the filter is better than that without the filter. The PSD of the surge control force, total displacement, and filtered displacement with application of the low pass filter are shown in Fig. 14. The frequency components of control forces are decided by the feedback states. Although there also exist the high frequency

Fig. 7 Time histories of displacements of the platform

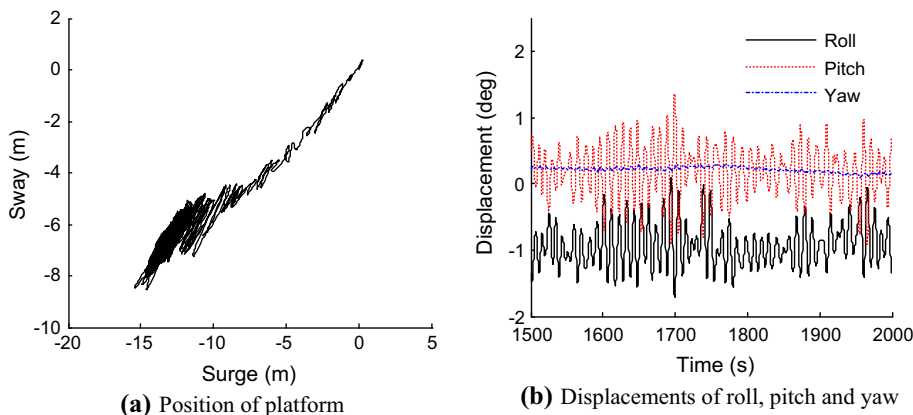


Fig. 8 Time histories of displacements of the platform

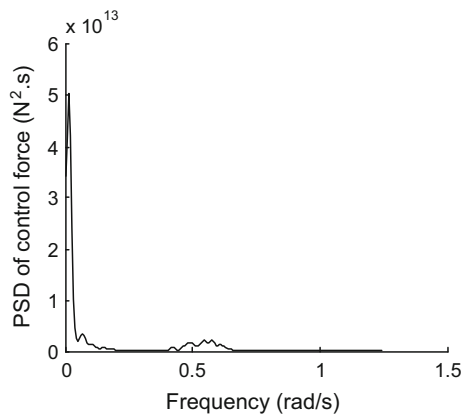
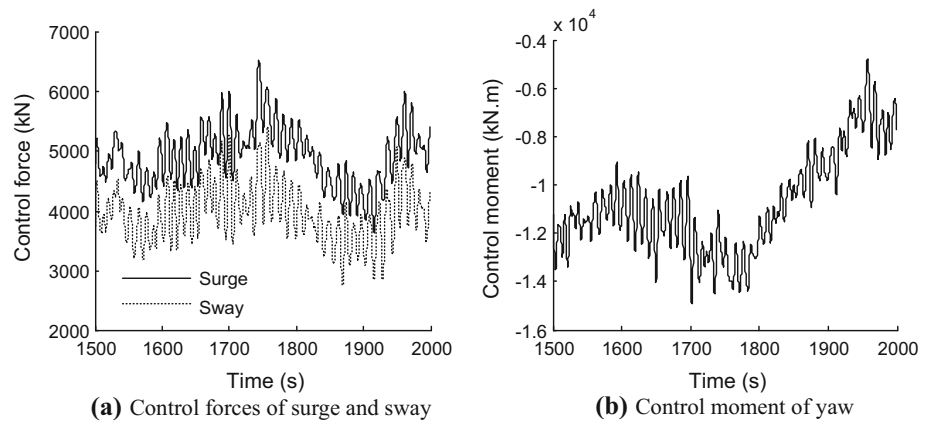


Fig. 9 PSD of surge control forces

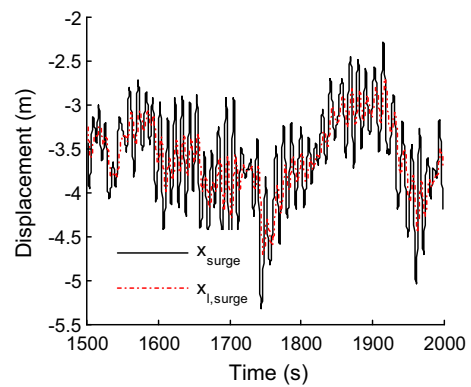


Fig. 11 Effects of low pass filter for the surge displacement: total displacement x_{surge} and filtered results $x_{l,surge}$

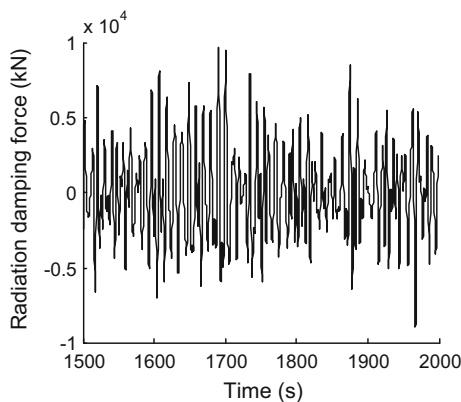


Fig. 10 The radiation damping forces of surge

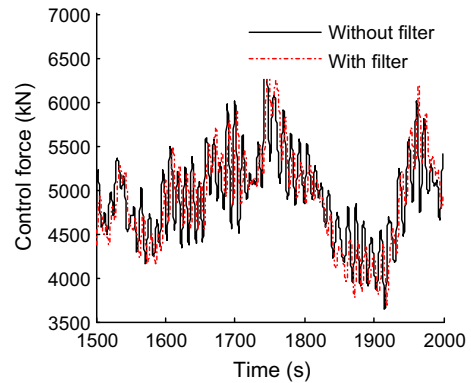


Fig. 12 Time histories of the two case's control force: 1 with filter (dotted line), 2 without filter (solid line)

components in the control forces, the proportion of the high frequency components is small and most of the control forces range in the low frequency area from zero to 0.2 rad/s.

The simulation results are also compared with the traditional controller design based on the 3-DOF model that considers only surge, sway, and yaw. The surge

displacements and surge control forces of both cases are shown in Figs. 15 and 16, respectively. The amplitudes of the control forces for the 3-DOF model controller approximately equal to the results of the fully coupled model. In 3-DOF control, both the wave-drift damping coupling terms and the hydrodynamic radiation damping coupling

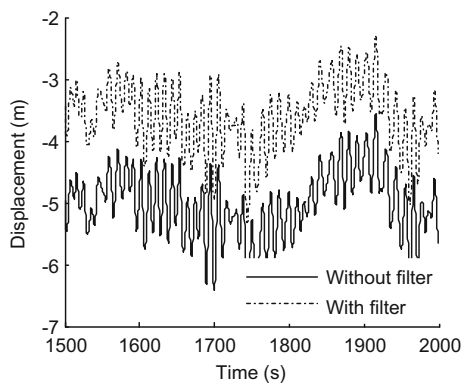


Fig. 13 Time histories of the two case’s surge displacement: **1** with filter (dotted), **2** without filter (solid)

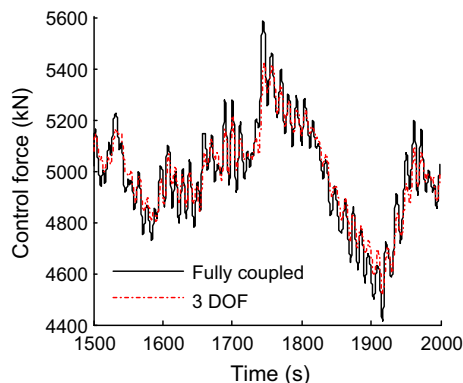


Fig. 16 Time histories of the surge control forces of the 3-DOF model and the fully coupled model

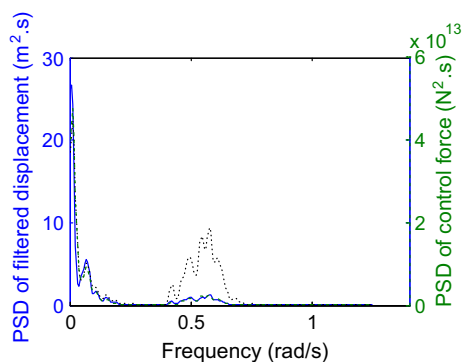


Fig. 14 The PSD of the control force (green line), filtered displacement $x_{1,surge}$ (blue line) and total displacement x_{surge} (black dotted line) (color figure online)

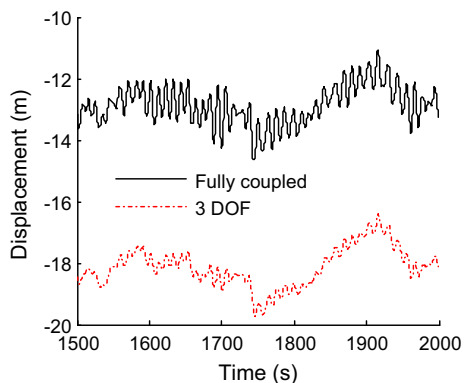


Fig. 15 Comparison of the surge displacements for the 3-DOF model and the fully coupled model

terms are neglected, so the surge displacement amplitude is significantly larger than that in the fully coupled result. If the same control performances of both cases are achieved, the amplitudes of the control forces from the 3-DOF model are obviously larger than the forces from the fully coupled model. The performance of the controller design based on

the 3-DOF model may be overly conservative for small-waterplane-area floating structures.

5 Conclusions

In this study, the fully coupled dynamic model derived from the Cummins equation is applied to design a DP controller for a semi-submersible platform. Using realization theory, the state-space models replace the convolution integral terms in the Cummins equation. Since only the displacements can be measured by the sensors, a static output feedback controller is constructed for the DP controller. The Lyapunov function is used to guarantee the stability, and then the L_∞ controller is obtained to reject persistent environmental disturbance. From the simulation results, the following conclusions can be obtained:

- The state-space model derived from the Cummins equation is a convenient and suitable means of designing the DP controller that avoids building the low frequency and wave frequency dynamic models separately. This model is sufficiently accurate to describe the platform dynamics in the controller design process.
- After the introduction of the low pass filter, the control performance is greatly improved because the filtered horizontal drift motions are the controlled outputs.
- Compared with the traditional 3-DOF model, when the amplitudes of the control forces are approximately equal, the surge displacement of the 3-DOF model is obviously larger than that of the model proposed here. Therefore, the coupling characteristics, mainly the radiation damping, cannot be neglected for a semi-submersible platform or other small-waterplane-area floating structure, and the performance of controller designs based on the 3-DOF model may be overly conservative.

Acknowledgments This work was financially supported by the National Fundamental Research Program of China (Program 973, Grant No. 2011CB013705) and the National Natural Science Foundation of China (Grant No. 51221961). The support is gratefully acknowledged.

References

- Sørensen JA (2011) A survey of dynamic positioning control systems. *Annu Rev Control* 35:123–136
- Perez T, Fossen TI (2011) Practical aspects of frequency-domain identification of dynamic models of marine structures from hydrodynamic data. *Ocean Eng* 38:426–435
- Tannuri EA, Kubota LK, Pesce CP (2006) Adaptive control strategy for the dynamic positioning of a shuttle tanker during offloading operations. *J Offshore Mech Arct* 128:203–210
- Tannuri EA, Agostinho AC, Morishita HM, Moratelli LJ (2010) Dynamic positioning systems: an experimental analysis of sliding model control. *Control Eng Pract* 18(10):1121–1132
- Fossen TI, Grøvlen A (1998) Nonlinear output feedback control of dynamically positioned ships using vectorial observer backstepping. *IEEE Trans Contr Syst Technol* 6(1):121–128
- Skjetne R, Fossen TI, Kokotovic PV (2005) Adaptive maneuvering, with experiments, for a model ship in a marine control laboratory. *Automatica* 41:289–298
- Girard AR, Empey DM, Webster WC, Hedrick JK (2003) An experimental testbed for mobile offshore base control concepts. *J Mar Sci Technol* 7(3):109–118
- Zhou L, Moan T, Riska K, Su B (2013) Heading control for turret-moored vessel in level ice based on Kalman filter with thrust allocation. *J Mar Sci Technol* 18(4):460–470
- Balchen JG, Jenssen NA, Mathisen E, Sælid S (1980) A Dynamic positioning system based on Kalman filtering and optimal control. *Model Identif Control* 1(3):135–163
- Sørensen AJ, Strand JP (2000) Positioning of small-waterplane-area marine constructions with roll and pitch damping. *Control Eng Pract* 8:205–213
- Cummins W (1962) The impulse response function and ship motions. *Schiffstechnik* 47:101–109
- Kristiansen E, Egeland O (2003) Frequency dependent added mass in models for controller design for wave motion ship damping. In: Proceedings of sixth IFAC conference on manoeuvring and control of marine craft MCMC'03, Girona, Spain
- Kristiansen E, Hjuslstad A, Egeland O (2005) State-space representation of radiation forces in time-domain vessel models. *Ocean Eng* 32:2195–2216
- McCabe A, Bradshaw A, Widden M (2005) A time-domain model of a floating body using transforms. In: Proceedings of the sixth European wave and tidal energy conference. University of Strathclyde, Glasgow
- Fossen TI, Smogeli ØN (2004) Nonlinear time-domain strip formulation for low-speed manoeuvring and station keeping. *Model Identif Control* 25(4):201–221
- Scherer C, Gahinet P, Ghilali M (1997) Multiobjective output-feedback control via LMI optimization. *IEEE Trans Autom Control* 42(7):896–911
- Chen H, Guo KH (2005) Constrained H_∞ control of active suspensions: an LMI approach. *IEEE Trans Control Syst Technol* 13(3):412–421
- Abedor J, Nagpal K, Poolla K (1996) A linear matrix inequality approach to peak-to-peak gain minimization. *IEEE Trans Robust Nonlinear* 6:899–927
- Jhi HL, Tseng CS (2012) Robust static output feedback fuzzy control design for nonlinear discrete-time systems with persistent bounded disturbances. *Int J Fuzzy Syst* 14(1):131–140
- Wu HN, Li HX (2009) Adaptive neural control design for nonlinear distributed parameter systems with persistent bounded disturbances. *IEEE Trans Neural Netw* 20(10):1630–1644
- Khosravi A, Jalali A (2008) A new LMI solution in the L_1 optimal problem for wind turbine-induction generator unit. *Appl Math Comput* 206:643–650
- Sadeghi MS, Momeni HR, Amirifar R (2008) H_∞ and L_1 control of a teleoperation system via LMIs. *Appl Math Comput* 206:669–677
- Ogilvie TF (1964) Recent progress toward the understanding and prediction of ship motions. In: The fifth symposium on naval hydrodynamics, pp 3–128
- Li YC, Teng B (2002) Wave action on maritime structures. Ocean press, Peking, pp 90–95 (in Chinese)
- Fossen TI (2005) A nonlinear unified state-space model for ship maneuvering and control in a seaway. *J Bifurc Chaos* 15(9):2717–2746
- Xiao-Fu JI, Hong-Ye SU, Jian CHU (2007) Peak-to-peak gain minimization for uncertain discrete systems: a matrix inequality approach. *ACTA Autom Sin* 33(7):753–756
- Boyd S, Ghaoui LE, Feronb E, Balakrishnan V (1994) Linear matrix inequalities in system and control theory. SIAM studies in applied mathematics, vol 15. SIAM, Philadelphia
- Löfberg J (2004) YALMIP: a toolbox for modeling and optimization in Matlab. In: Proceedings of IEEE symposium on computer-aided control system design, Taipei, Taiwan
- Kocvara M, Sting M (2006) PENBMI user's guide. <http://www.penopt.com>
- Herion D, Löfberg J, Kocvara M, Sting M (2005) Solving polynomial static output feedback problems with PENBMI. In: Proceedings of conference on decision and control, and European control conference, Sevilla, Spain, pp 7581–7586
- Zhu H (2011) Studies on the motion performance of a semi-submersible platform and the heave motion damping system using moveable heave-plate. Harbin Institute of Technology, Harbin, pp 57–62
- DNV-OS-E301 (2010) Position mooring. Det Norske Veritas, Høvik, pp 32–34
- Sørensen AJ (2012) Marine control systems: propulsion and motion control of ships and ocean structures. Lecture notes. Department of Marine Technology, NTNU